Merger History of Halos in Excursion Set Theory Approach

Arefe Abghari, Setareh Foroozan

Contents

1 Introduction

The formation of cosmological structures is explained by hierarchical structure formation, in which, structures form by amplification of tiny fluctuations. In studying the formation and evolution of cosmological structures the non-linear regime is crucial, for there is no analytical solution for the equations. In order to connect the initial perturbations to the nonlinear structures we see today, one has to understand the outcome of nonlinear evolution. Excursion Set Theory (EST) is a powerful approach to investigate the statistical properties of halos such as growth rate in the non-linear regime.

In the second section we will review structure formation in the standard paradigm. The third section is devoted to spherical collapse model. In sections 4 and 5 we introduce Press-Schechter formalism and Excursion Set Theory respectively. Finally in the last section we present the preliminary results of our own analysis.

2 A Brief Review on Structure Formation

In this section, we briefly review the features of initial perturbation field and the evolution of perturbations in the linear regime.

According to the benchmark model, dark matter halos form through gravitational instability. Density perturbations grow linearly until they reach a critical density, after which they turn around from the expansion of the Universe and collapse to form virialized dark matter halos. These halos continue to grow in mass (and size), either by accreting material from their neighborhood or by merging with other halos. Some of these halos may survive as bound entities after merging into a bigger halo, thus giving rise to a population of subhalos.

In a perfectly homogeneous and isotropic universe, structure formation will never take place. Therefore, an initial perturbation field should be supposed. In the benchmark model of structure formation, small perturbations are generated during the inflation era; they grow by the expansion of universe until they become large enough to get amplified through gravitational instability i.e. non-linearly.

2.1 Density field and power spectrum of matter

Density contrast is a useful parameter for characterizing perturbations. It is defined by,

$$\delta(\mathbf{x}, t) \equiv \frac{\rho(\mathbf{x}, t) - \bar{\rho}(\mathbf{x}, t)}{\bar{\rho}(\mathbf{x}, t)}$$

It indicates where there are local enhancements in matter density. The random field is characterized by the joint probability distribution,

$$P(\delta(x_1), \delta(x_2), \delta(x_3), ...)d\delta(x_1)d\delta(x_2)...$$

This distribution can only be completely determined by having all of its moments. However, in the standard paradigm, the initial density fluctuation is supposed to be a realization of a Gaussian random field generated from the cosmological inflation; this means that the joint probability distribution of density contrast at a set of points in space is given by a multivariate Gaussian random field. Therefore it can be determined by its first and second moments. Since only one realization of the field is available, using the Ergodic theory, we need to take averages on space instead of averaging on ensemble.

By definition, the first moment of this field vanishes. For a Gaussian random field the N-point correlation function can be determined by two-point correlation function; therefore we only need to evaluate the two-point function. The two-point correlation function is defined by

$$\xi(\mathbf{r}) = \langle \delta(\mathbf{x})\delta(\mathbf{x}+\mathbf{r}) \rangle$$

Due to isotropy, the two-point correlation is only a function of $|\mathbf{r}|$ and it does not depend on its direction. Taking the Fourier transform gives

$$\langle \tilde{\delta}(k)\tilde{\delta}(k') \rangle = \int d^n x e^{-ix\cdot k} d^n y e^{ix\cdot k} \langle \delta(x)\delta(x') \rangle = (2\pi)^n \delta(k-k') P_\delta(k)$$

where $P_\delta(k)$ is the power spectrum, the Fourier transform of the two-point correlation function. The power spectrum has dimensions of volume, so we can define a more useful dimensionless combination

$$\Delta^2(k) \equiv \frac{k^3}{2\pi^2} P(k)$$

As a result, to characterize the initial Gaussian field, we need the two-point correlation function or equivalently the power spectrum.

An overdensity field $\delta(\mathbf{x}; R)$ which is a smoothed version of $\delta(\mathbf{x})$ is defined by

$$\delta(\mathbf{x}', R_W) \equiv \int d^3 x' W(|\mathbf{x}' - \mathbf{x}|, R_W)\delta(\mathbf{x})$$

We can find the Fourier transform of window function and density contrast accordingly.

2.2 Linear perturbation theory

As discussed in the previous section, the initial density field is supposed to be homogeneous and isotropic with tiny fluctuations around the average. Therefore we can suppose that these fluctuations are caused by the perturbations in the energy-momentum tensor of a homogeneous background. We can linearize the Einstein equation to reach a second order differential equation; eventually, we can study each Fourier mode of the density contrast independently.

The proper way to study the Dark Matter (DM) is through collisionless Boltzmann equation. However in large scale, deviations from fluidity are negligible and we can use fluid approximation. The fluid equations for vanishing pressure are included below:

$$Continuity: \qquad \frac{\partial \rho(\mathbf{r},t)}{\partial t} + \nabla_r \cdot [\rho \mathbf{u}(\mathbf{r},t)] = 0 \tag{1}$$

$$Euler: \qquad \frac{\partial \mathbf{u}}{\partial t} + (\mathbf{u}\cdot\nabla_r)\mathbf{u} = -\nabla_r \phi \tag{2}$$

$$Poisson: \qquad \nabla_r^2 \phi = 4\pi G\rho - \Lambda \tag{3}$$

After transforming these equations into co-moving coordinate ($\mathbf{r}$ = a(t)$\mathbf{x}$) and linearizing in δ, the three perturbation equations become

$$\frac{\partial \delta}{\partial t} + \frac{1}{a}\nabla_x \cdot \mathbf{v} = 0 \tag{4}$$

$$\frac{\partial \delta}{\partial t} + \frac{\dot{a}}{a}\mathbf{v} = -\frac{1}{a}\nabla_x \phi \tag{5}$$

$$\nabla_x^2 \phi = \frac{3H_0^2 \Omega_m}{2a}\delta \tag{6}$$

Combining the time derivative of the linearized continuity equation and divergence of linearized Euler equation together with Poisson equation gives

$$\boxed{\frac{\partial^2 \delta}{\partial t^2} + 2\frac{\dot{a}}{a}\frac{\partial \delta}{\partial t} \frac{3H_0^2\Omega_m}{2a^3}\delta = 0} \tag{7}$$

Here we derive the same equation for the Fourier transform $\tilde{\delta}$. This is an ordinary second order differential equation, and its solution can be written as

$$\delta(\mathbf{x},t) = D_+(t)\Delta_+(\mathbf{x}) + D_-(t)\Delta_-(\mathbf{x}) \tag{8}$$

$H(t) = \frac{\dot{a}}{a}$ is a solution to Equation 7 for a matter dominated era, where pressure vanishes. This is proportional to the decaying solution. The second solution of the differential equation can be derived from the first solution. One can find

$$D_+(t) \propto \frac{5\Omega_m}{2} \frac{H(a)}{H_0} \int_0^a \frac{da'}{[\Omega_m a'^{-1} + \Omega_\Lambda a'^2 + (1 - \Omega_m - \Omega_\Lambda)]^{3/2}} \tag{9}$$

The above integral can not be calculated analytically for $\Omega_\Lambda \neq 0$, therefore we evaluated it numerically as a function of redshift (z); still, $D_+(t)$ should be normalized to unity for the present time. The plot is shown in Figure 1

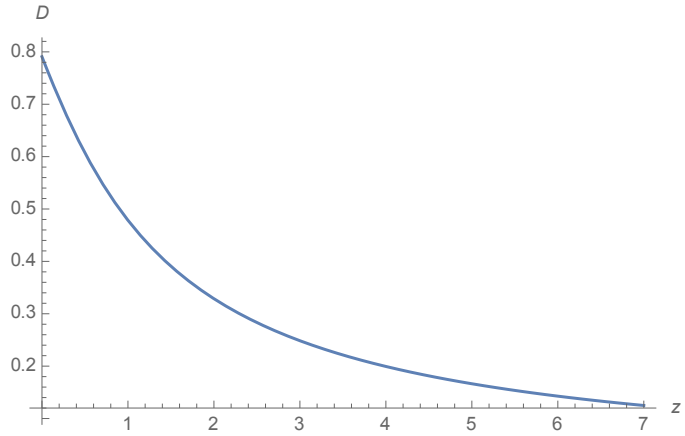

Figure 1: Growth function D(z) with respect to z. The values then were normalized to one.

3 Spherical Collapse

Many objects in the present-day Universe, including galaxies and clusters of galaxies, have densities orders of magnitude higher than the average density of the Universe. These objects are thus in the highly nonlinear regime, where $\delta >> 1$. To complete our description of structure formation in the Universe, we therefore need to go beyond perturbation growth in the linear and quasi-linear regimes, discussed in the previous section, and address the gravitational collapse of overdensities in the nonlinear regime.

In this section, we study the nonlinear gravitational collapse in which non-gravitational effects are negligible. In general, nonlinear gravitational dynamics is difficult to deal with analytically, however if simple assumptions are made about the symmetry of the system, analytical models can still be constructed. Although these models are not expected to give accurate descriptions of the true nonlinear

problem of gravitational collapse, they provide valuable insight into the complex processes involved. One practical model is spherical model, which studies the collapse of a spherical region with mean density contrast $\bar{\delta}$ in a pressureless matter dominated universe. We are interested in modes that are smaller than the Hubble radius, greater modes should be studied differently. With these assumptions, Newtonian approximation is valid. We start with the Newtonian equation,

$$\frac{d^2r}{dt^2} = -\frac{GM}{r^2} \tag{10}$$

Integrating this equation gives

$$\frac{1}{2}(\frac{dr}{dt})^2 - \frac{GM}{r} = E \tag{11}$$

where E is the energy of the shell. Here, we assume that no shell-crossing happens during the collapse i.e. the mass inside each shell is constant. For a gravitational system to be closed, the energy should be negative. The physical radius is shown by r, which is written in the co-moving coordinate as $\mathbf{r} = a(t)\mathbf{x}$. It can be easily deduced that the solution to Equation 11 is given as below

$$r = A(1 - cos\theta) \tag{12}$$

$$t = B(\theta - sin\theta) \tag{13}$$

And we have

$$A^3 = GMB^2 \tag{14}$$

In which A and B are constants, with the boundary condition that at $r = r_{max}$, $\dot{r} = 0$ and substituting in Equation 10, we see that A and B are given by

$$A = \frac{GM}{2|E|} \tag{15}$$

$$A^3 = GMB^2 \tag{16}$$

$$B = \frac{GM}{(2|E|)^{3/2}} \tag{17}$$

In the first two leading orders,

$$r(\theta) = A(\frac{\theta^2}{2} - \frac{\theta^4}{24}) \tag{18}$$

$$t(\theta) = B(\frac{\theta^3}{6} - \frac{\theta^5}{120}) \tag{19}$$

$$\tag{20}$$

Therefore in the leading order $r = \frac{A}{2}(\frac{6t}{B})^{3/2}$.

By iterating,

$$\theta \approx (\frac{6t}{B})^{1/3}[1 + \frac{1}{60}(\frac{6t}{B})^{2/3}]$$

Substituting back into r gives:

$$r(\theta) \approx \frac{A}{2}(\frac{6t}{B})^{2/3}[1 - \frac{1}{20}(\frac{6t}{B})^{2/3}] \tag{21}$$

Substituting this into the expression for density $\rho = \frac{M}{4/3\pi r^3}$ and using Equation 16 gives the following result for density,

$$\frac{1}{6\pi t^2 G}(1 + \frac{3}{20}(\frac{6t}{B})^{2/3}) \tag{22}$$

from which one can read the density contrast;

$$\delta = \frac{3}{20}(\frac{6t}{B})^{2/3} \tag{23}$$

For the matter dominated era we have:

$$t = \frac{2}{3H_0\Omega_m^{1/2}}a^{3/2} \tag{24}$$

which gives

$$\delta = \frac{3}{20}a(\frac{4}{BH_0\Omega_m^{1/2}})^{3/2} \tag{25}$$

from which one can read A and B as follows:

$$B = \frac{1}{2H_0\Omega_m^{1/2}}(\frac{3a_i}{5\delta_i})^{3/2} \tag{26}$$

$$A = \frac{3a_i}{10\delta_i} \tag{27}$$

in which the subscript i means initial. Solving for the scale factor at collapse ($\theta = 2\pi$) gives the following result:

$$a_{collapse} = (\frac{3}{4})^{2/3}(\frac{3a_i}{5\delta_i}) = 1.686\ \frac{a_i}{\delta_i} \tag{28}$$

In this model, the collapsing time is infinite; thus we need to extrapolate to get the value of 1.686 for the critical density of the present time. If an overdense region passes the critical density, it will collapse. The critical density at a desired time

can be derived from the present time critical density divided by growth function: $\delta_c(z) = \delta_c(0)/D(z)$.

Therefore, we do not need the physical constraint $\delta > -1$ since it is the extrapolation of a much smaller value.

The collapse continues until the structure becomes virialized. At this time, the radius of this structure is equal to A. The collapse time is $t = 2\pi B$. For the density contrast of a virialized object we have

$$\delta \approx \frac{\rho}{\bar{\rho}} = 18\pi^2 \approx 178$$

Finally, the density contrast of a virialized object is approximately 200.

4 Press–Schechter Formalism

According to the spherical collapse model, regions with $\delta(x, 0) > \delta_c(0) \approx 1.69$, or equivalently, with $\delta(x, t) > \delta_c/D(t)$, will have collapsed to form virialized objects. Suppose that the probability of collapse for a region is given by F(M). It is given by the cumulative probability that this region has the smoothed density above the threshold δ_c

$$F(M) = \int_{\delta_c}^{\infty} P(\delta; R) d\delta \tag{29}$$

From which the mass function can be deThe mass s function can then be wririved atten as

$$n(M)dM = \frac{\rho_M}{M} |\frac{dF}{dM}| dM \tag{30}$$

If $\delta_0(x)$ is a Gaussian random field then so is $\delta_s(x)$, and the probability that $\delta_s > \delta_c(t)$ is given by

$$P[> \delta_c] = \frac{1}{\sqrt{2\pi}\sigma(M)} \int_{\delta_c}^{\infty} \exp\left(-\frac{\delta_s^2}{2\sigma^2(M)}\right) d\delta_s \tag{31}$$

Here

$$S \equiv \sigma^2(M) = \langle \delta_s^2(\boldsymbol{x}, \boldsymbol{R}) \rangle = \frac{1}{2\pi^2} \int_0^{\infty} P(k) \tilde{W}^2(\boldsymbol{k}R) k^2 dk \tag{32}$$

Where S the variance of the density perturbation field, is a monotonic function of R. Equation 31 has an analytical solution for a window function that is constant value over a range. This window function is called k-sharp window. According to

the PS ansatz, the probability $P[> M]$ is equal to $F(> M)$, the mass fraction of collapsed objects with mass greater than M. There is, however, a problem here. As $M \longrightarrow 0$, then $\sigma(R) \longrightarrow \infty$ (at least for a power-law spectrum with $n > 3$) and $P[> \delta_c(t)] \longrightarrow 1/2$. This would suggest that only half of the mass in the Universe is part of collapsed objects of any mass. This is a characteristic of linear theory, according to which only regions that are initially overdense can form collapsed objects. However, underdense regions can be enclosed within larger overdense regions, giving them a finite probability of being included in a larger collapsed object. This is one plausible manifestation of the cloud-in-cloud problem. This problem was first addressed by introducing an extra factor of 2. Then, using EST, this factor was justified.

Having Gaussian random field and sharp k-space filter, we can obtain the solution to diffusion equation. Afterwards, we obtain the fraction of trajectories with a first upcrossing at $S > S1$,

$$f_{FU}(S, \delta_c) = \frac{\delta_c}{\sqrt{2\pi} S^{3/2}} exp[-\frac{\delta_c^2}{2S}] \tag{33}$$

This function is plotted in Figure 2 to be compared with the function obtained from EST. (the algorithm will be explained later).

5 Excursion Set Theory

Excursion Set Theory is a numerical approach to determine the distribution of regions that can develop to become a virialized object. It was first introduced by Bond et al. (4) as an extension to Press-Schechter method. In the excursion set approach, we consider $\delta(x; R)$ for a single point in space. We need to find the largest radius (smallest density variance) in which the smoothed mass density exceeds the critical density. This region will collapse and form an object with mass of given by the size of region. The number density of halos with specific mass then is related to the probability that a trajectory passes the critical density at the corresponding S. This is equivalent to F(M) in Equation 29, so the mass function can be derived by generating several trajectories and finding the first up-crossing probability, then Equation 30 gives mass function. The first up-crossing distribution for k-sharp (Markovian) and top-hat (non-Markovian) window function are shown in Figure 2. As it can be seen, the Markovian distribution is in agreement with PS distribution given in Equation 29.

In the next section, we provide an important point regarding EST and then in the following sections, we explain how the trajectories are generated.

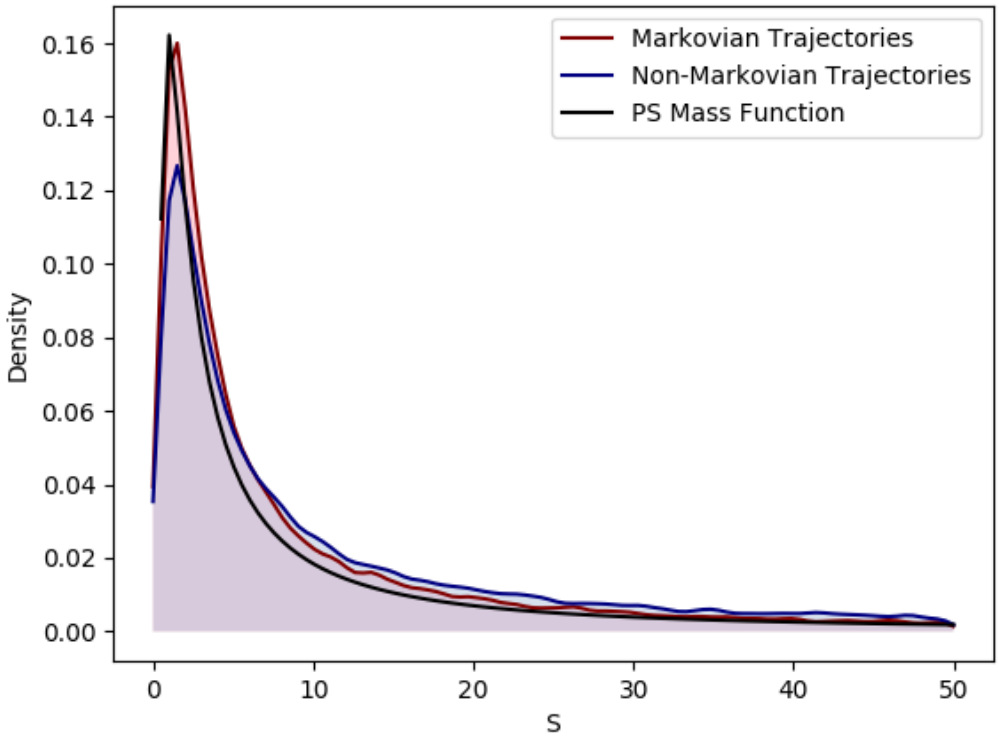

Figure 2: First up-crossing histogram for top-hat window function. The y axis is the fraction of trajectories that have their first up-crossing in the range (S,S+dS). The analytic PS mass function is shown for comparison.

5.1 Interpretation of the excursion set

In deriving the halo mass function using the excursion set formalism, we have made the ansatz that the fraction of trajectories with a first up-crossing on a mass scale (M, M + dM) is equal to the mass fraction of the Universe in collapsed objects with masses in this range. However, a simple example suggests that the mass associated with the first up-crossing of a mass element is only a lower limit on the actual mass of the collapsed object to which the mass element belongs. Thus, the ansatz on which the EPS formalism is based cannot be correct for individual mass elements. Yet, the resulting mass function seems to be in good agreement with numerical simulations. This paradox is often interpreted as indicating that the excursion set formalism predicts, in a statistical sense, how much mass ends up in collapsed objects of a certain mass at a given time, but that it cannot be used to predict the halo mass in which a particular mass element ends up.

5.2 Markovian trajectories

We fix the statistical distribution of the density contrast by the window function. One simple choice of window function from which the distribution of density contrast can be derived is k-sharp window.

$$\tilde{W}(k,R) = \left\{ \begin{array}{c} 1 \text{ for } k < 1/R \\ 0 \text{ for } k > 1/R \end{array} \right\}$$

The two-point correlation function is then given by

$$\langle \delta_i \delta_j \rangle = C_{ij} = \int \frac{dk}{k} \frac{k^3 P(k)}{2\pi^2} \tilde{W}(k;R_i)\tilde{W}(k;R_j) \tag{34}$$

Where P(k) is the power spectrum, is the Fourier transform of the window function, and $C_{ij} = S_i$ is the variance of δ when smoothed on scale R_i. In our analysis we estimated P(k) function with $P(k) = Ak^{-2}$ where A is a constant, therefore we can derive the correlation matrix

$$C_{ij} = \frac{A}{2\pi^2} \int dk \tilde{W}(kR_i)\tilde{W}(kR_j) \tag{35}$$

$$= \frac{A}{2\pi^2} * \frac{1}{R_i} if R_i > R_j \tag{36}$$

$$= \frac{A}{2\pi^2 max(R_i, R_j)} \tag{37}$$

Therefore we can calculate all the elements of correlation matrix as following:

$$S(R) = C_{ii} = \frac{A}{2\pi^2 R} \tag{38}$$

$$C_{ij} = min(S(R_i), S(R_j)) \tag{39}$$

5.3 Non-Markovian trajectories

Now it is the time to assume a more realistic smoothing window function to reach non-Markovian trajectories. We choose the top-hat window function

$$W(x,R) = \left\{ \begin{array}{c} \frac{3}{4\pi R_W^3} \text{ for } x < R_w \\ 0 \text{ for } x > R_W \end{array} \right\}$$

$$\tilde{W}(k,R) = 3\frac{sin(kR) - kRcos(kR)}{(kR)^3} \tag{40}$$

$$C_{ij} = \frac{A}{2\pi^2} \int dk \tilde{W}(kR_i)\tilde{W}(kR_j) \tag{41}$$

$$= \frac{9A}{240\pi} * \frac{10R_i^2R_j^3 - 2R_j^5}{R_i^3R_j^3} \; if \; R_i > R_j \tag{42}$$

Therefore we can calculate all the elements of correlation matrix

$$S(R) = C_{ii} = \frac{A}{30\pi R} => S = \frac{3A}{10\pi R} \tag{43}$$

The relation between S and R derived here and also in Equation 38 gives the relation between S and M in each case.

$$C_{ij} = \frac{S(R_i)}{4}[5 - \frac{S(R_i)^2}{S(R_j)^2}] \tag{44}$$

5.4 Cholesky decomposition

In this section, we explain how trajectories with correct statistical properties are generated. This discription is heavily based on (5). $C_{ij} = \langle \delta_i \delta_j \rangle$, the covariance between walk heights on scales S_i and S_j is useful in this procedure. The matrix C is real, symmetric, and positive-definite, so it has a unique decomposition $C = LL^T$, in which L is a lower triangular matrix. This decomposition is known as Cholesky's decomposition. We use L to generate the ensemble of trajectories as follows: First, consider a vector ξ, which is Gaussian white noise with zero mean and unit variance (i.e. $\langle \xi_m \xi_n \rangle = \delta_{mn}$). If we generate our desired trajectories as

$$\delta_i = \sum_j L_{ij}\xi_j \tag{45}$$

then the δ_i will have correlations between heights given by:

$$\langle \delta_i \delta_j \rangle = \sum_{m,n} L_{im}L_{jn}\langle \xi_m \xi_n \rangle = LL^T = C \tag{46}$$

Since L is triangular, each δ_i only requires a sum over $j <= i$, which makes this method faster.

5.5 Conditional trajectories

Consider a spherical region with mass M_2 which is formed a collapsed object at time t_2. We are interested in the fraction M_1 that was collapsed at time $t_1 < t_2$. So we need to calculate the probability that a random walk passing from (S_1, δ_1)

to execute a first up-crossing of the barrier δ_2 at S_2 corresponding to M_1. The conditional mass function is the average number of halos of mass M_2 at time t_2, that were a collapsed object of mass M_1 at time t_1. This is given by

$$\frac{dn(M_2|M_1)}{dM_2} = \frac{M_1}{M_2} f(S_2, \delta_2|S_1, \delta_1)|\frac{dS_2}{dM_2}|$$

This can be viewed as a two-barrier problem and will be calculated using EST formalism. In the extended Press-Schechter formalism in which walks are Markovian, the probability is simply given by Gaussian distribution with parameters $(\delta_1 - \delta_0, S_1 - S_0)$. However, in non-Markovian distribution, the conditional probability distribution cannot be driven analytically and we need to generate trajectories that pass through the desired point. It helps us choose halos of a particular mass in the present time.

Let X and Y be two random variables with probability density function p(x,y). If $< Y|X = x >$ is a linear function of $\tilde{x}$, that is, if $< Y|X = x^\star >= \alpha\tilde{x} + \beta$ for some $\alpha, \beta \in R$, then,

$$\langle Y|X = x^\star\rangle = \langle Y\rangle + \rho\frac{\sigma_Y}{\sigma_X}(x^\star - \langle X\rangle) \tag{47}$$

where in this equation,

$$\rho = \frac{Cov(X,Y)}{\sigma_Y \sigma_X} \tag{48}$$

Secondly, let p(x,y) be the joint probability density function of continuous random variables X and Y . $\langle Y|X = x\rangle$ is a linear function of and $\sigma_{Y|X=x}^2$ is constant, then,

$$\sigma^2_{Y|X=x^\star} = (1 - \rho^2)\sigma_Y^2 \tag{49}$$

In our case the random variable Y is $\delta(S)$ and X is $\delta(S_0)$; and our condition specifies that $x^\star = \Delta_0$ Therefore the mean value of the density contrast reads as

$$\langle\delta(S)|\delta(S_0) = \Delta_0\rangle = \frac{\Delta_0}{S_0}\langle\delta(S)\delta(S_0)\rangle$$

The parameter we want to evaluate is the conditional correlation function;

$$\langle\delta(S) - \langle\delta(S)|\delta(S_0) = \Delta_0\rangle\rangle\langle\delta(S') - \langle\delta(S')|\delta(S_0) = \Delta_0\rangle\rangle =$$

$$\langle\delta(S)\delta(S')\rangle - \langle\langle\delta(S)\delta(S_0)\rangle\frac{1}{S_0}\delta(S_0)\delta(S')\rangle -$$

$$\langle\langle\delta(S')\delta(S_0)\rangle\frac{1}{S_0}\delta(S_0)\delta(S)\rangle+$$

$$\frac{1}{S_0^2}\langle\delta(S)\delta(S_0)\rangle\langle\delta(S')\delta(S_0)\rangle\langle\delta(S_0)^2\rangle =$$

$$= \langle\delta(S)\delta(S')\rangle - \frac{1}{S_0}\langle\delta(S)\delta(S_0)\rangle\langle\delta(S_0)\delta(S')\rangle \tag{50}$$

In the above derivation we used the fact that the mean of the two random variables are zero. A set of non-Markovian trajectories generated using this method with condition for passing from $\delta = 1.686$, $S = 1$ is shown in Figure 3.

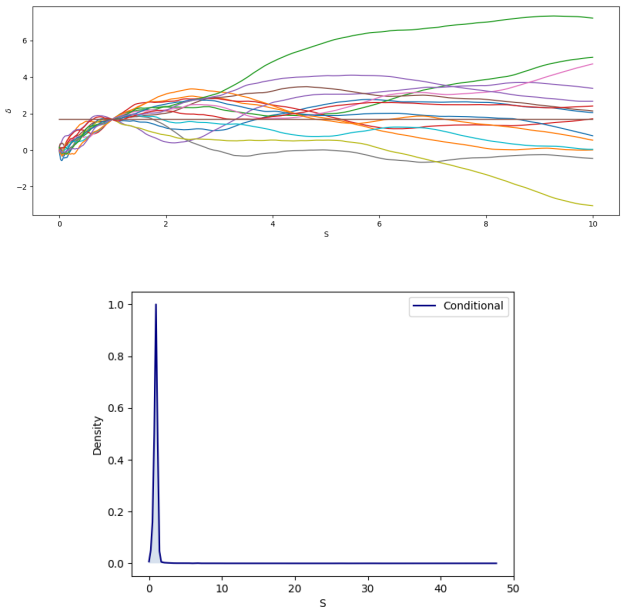

Figure 3: Up: a schematic representation of non-Markovian trajectories in (S, δ_s) space. Each trajectory corresponds to a mass element in the initial (Gaussian) density field, and δ_s is the overdensity at the location of that mass element when the initial density field, linearly extrapolated to the present time, is smoothed with a top-hat filter of mass M given by $S = \sigma^2(M)$. All of the trajectories are forced to pass through a certain point $S_0 = 1$ and $\delta_0 = 1.686$. Down: first up-crossing histogram for conditional trajectories. The y axis is the fraction of trajectories that have their first up-crossing at S_0.

In order to check our statistics and algorithm, we generated Markovian conditional trajectories and the histogram of their δ value in a certain S, which is shown in Figure 4.

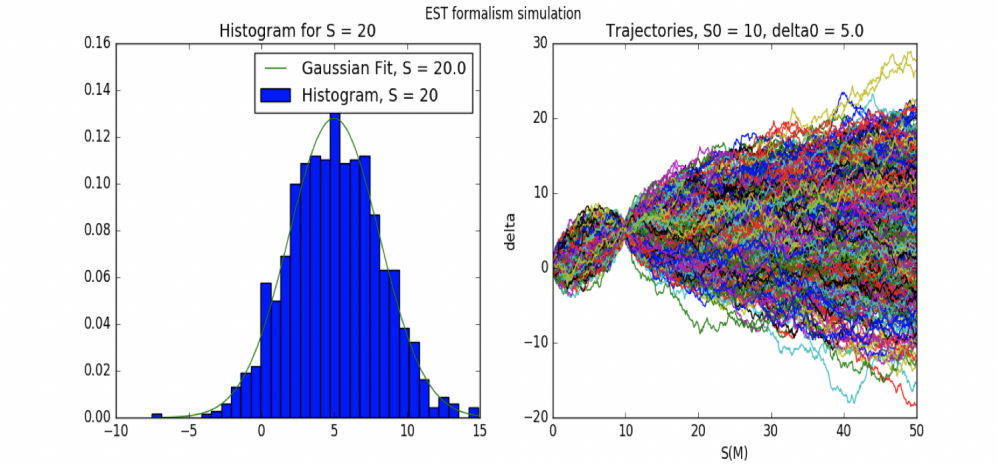

Figure 4: 1000 conditional Markov trajectories generated by Cholesky decomposition. To test our method, the distribution of δ is drawn and the standard deviation is computed. It clearly follows the Gaussian distribution as expected.

5.6 Merger tree

One of the advantages of the EST formalism is that it provides a clear way to calculate the properties of the progenitors which give rise to a given class of collapsed objects. For example, one can calculate the mass function at z = 5 of those halos (progenitors) which by $z_0 = 0$ end up in a massive cluster-sized halo of mass M_0. Thus, the EST formalism allows one to describe how a dark matter halo assembled its mass via mergers of smaller mass halos.

The merger history for a halo can be represented pictorially by a merger tree such as that shown in Figure 5. In this plot, redshift increases from left to right and the horizontal axis shows the mass of halo. To this end, we first find the critical density for each redshift bin, and then the mass (first up-crossing point) of each halo for each redshift bin. Having mass of the halos for all redshift bins, we can plot mass versus redshift, the so called merger tree. Merger trees for both k-sharp and top-hat functions are shown in Figure 5. Observe that the power of this approach lies in the statistics; that is, one merger tree does not convey any information about halos, one should generate several merger trees and study the likelihood of the desired property.

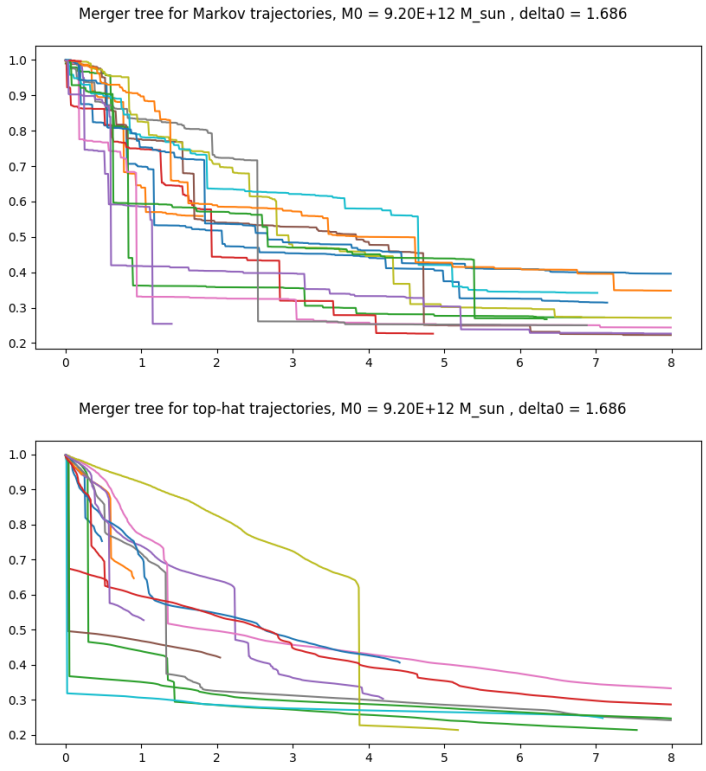

Figure 5: Merger history generated using k-sharp window function (up) and top-hat window (down). The conditional statistics have been used to fix the present mass of halos. It is believed that the smooth rise in the mass of merger trees is caused by accretion; on the other hand, the parts with steep slopes are due to sudden mass gain through a merge with another halo.

6 Results

6.1 Fossil groups

A very interesting quantity is merging rate and accretion rate in halos. Since EST has been very successful in describing the number density of halos in the standard cosmological paradigm (ΛCDM), one can also apply it to other cosmological models. Using EST instead of simulating the whole Universe again is advantageous, for simulations do consume much more time.

In this project, we aimed to study the number density of fossil groups with EST approach. Fossil galaxy groups are believed to be the end result of galaxy-galaxy merging. The time-scales for dynamical friction on luminous galaxies suggest that fossil groups are old, undisturbed systems that have seen little infall of L* galaxies since their initial collapse. Fossil groups are thus an important laboratory for studying the formation and evolution of galaxies and the intragroup medium in an isolated system. Fossil groups may still contain unmerged dwarf galaxies, but the more massive members of the group have condensed into the central galaxy.

In our investigation, we computed the redshifts in which, each halo gained 50% and 90% of its final mass. The difference between these two redshifts is denoted by Δz. In a fossil group, we expect the the halo to go through its path from 50% to 90% in a short period of time; in other words, Δz must be small. Histograms of 50% and 90% mass gain redshift and Δz are shown in Figure 6 Therefore in the next step, to study their statistics, we will choose halos with small Δz and large formation time.

6.2 Merger history and formation time distribution

In a recent N-body simulation, (8), Shi et al. introduced a parameter $a_{nf} = \frac{1+z_{form}}{1+z_{peak}}$ that characterizes the ratio of maximum mass time (in our study, z_{peak} is the redshift of the time that a subhalo merged for the last time, thus we refer to it as last merging redshift) with respect to formation time of galaxy halos. The histogram of a_{nf} shows a bimodal distribution. Based on this bimodality, they concluded that at a given z_{peak}, infall halos are dominated by a young population at low redshift and an old population at high redshift. The distribution is shown in Figure 7. This bimodality could be suggesting a connection to color and Star Formation Rate (SFR) of galaxies. They examined this distribution with the EST formalism using Markov walks, but it did not show bimodal distribution. They pointed out that it might be caused by the fact that EPS approach does not consider environmental effects. Here we examined this distribution using a real top-hat window function which is represents a non-Markovian path. The following is a list of our main results:

- Since we expect that mass growth through merging is faster than accretion, we can roughly say that sudden drops in a merger tree corresponds to merge. Based on this, we set a threshold on the slope of merger trees and classified each point above this threshold as merging. To calculate the slope of merger trees and for fixing the threshold, we adopted several methods, however it seems that the shape of a_{nf} distribution is independent from these variant choices.

- We plotted the distribution for three different halo masses; 10^{11}, 10^{12}, and 10^{13} M_{sun}. Again, there is no significant difference in their a_{nf} distribution.

- As you can see in Figure 8, we see a narrow peak at $a_{nf} = 1$. By examining trees in this region, it seems that they gain most of their mass through their first merging and therefore a_{nf} for those paths is exactly equal to one (up to our precision), but other trees gain 50% of their mass far from their last-merging mass. Thus, we need to explain why these trees are spread in such a narrow peak, which we will refer to as the "suspicious peak". However, ignoring this peak, we clearly do not see any bimodality.

- Shi et al. in (8) observed that for halos with small z_{peak} (recently merged halos), the second peak in a_{nf} distribution is wider. In our analysis, we can see similar effect when we choose halos with small last-merge redshifts.

- We plotted this diagram for Markov trajectories with $10^{14} M_{sun}$. The general shape is similar to the one for non-Markov trajectories, however, in the Markov diagram the suspicious peak is shorter.

- Comparing the formation distribution with the distribution of Δz for fossil groups, we can see that they are almost the same. Both have the "suspicious peak", and the main peak for both is around z = 2. Since they are both a measure of formation time, generated by different algorithms, they are expected to be in consistency.

References

[1] Houjun Mo, Frank van den Bosch and Simon White, Galaxy Formation and Evolution.

[2] T. Padmanabhan, Structure Formation in the Universe

[3] S. Dodelson, "Modern Cosmology," Amsterdam, Netherlands: Academic Pr. (2003) 440 p

[4] Bond J., Cole S., Efstathiou G., Kaiser N., 1991, ApJ, 379, 440

[5] F. Nikakhtar et al. "The Excursion set approach: Stratonovich approximation and Cholesky decomposition," [arXiv:1802.04207 [astro-ph.CO]].

[6] A. R. Zentner, "The Excursion Set Theory of Halo Mass Functions, Halo Clustering, and Halo Growth," [astro-ph/0611454].

[7] S. Baghram et al. "Exact enumeration approach to first-passage time distribution of non-Markov random walks," [arXiv:1906.02081 [cond-mat.stat-mech]].

[8] J. Shi et al., 2017, arXiv:1712.00324v2[astro-ph.CO]

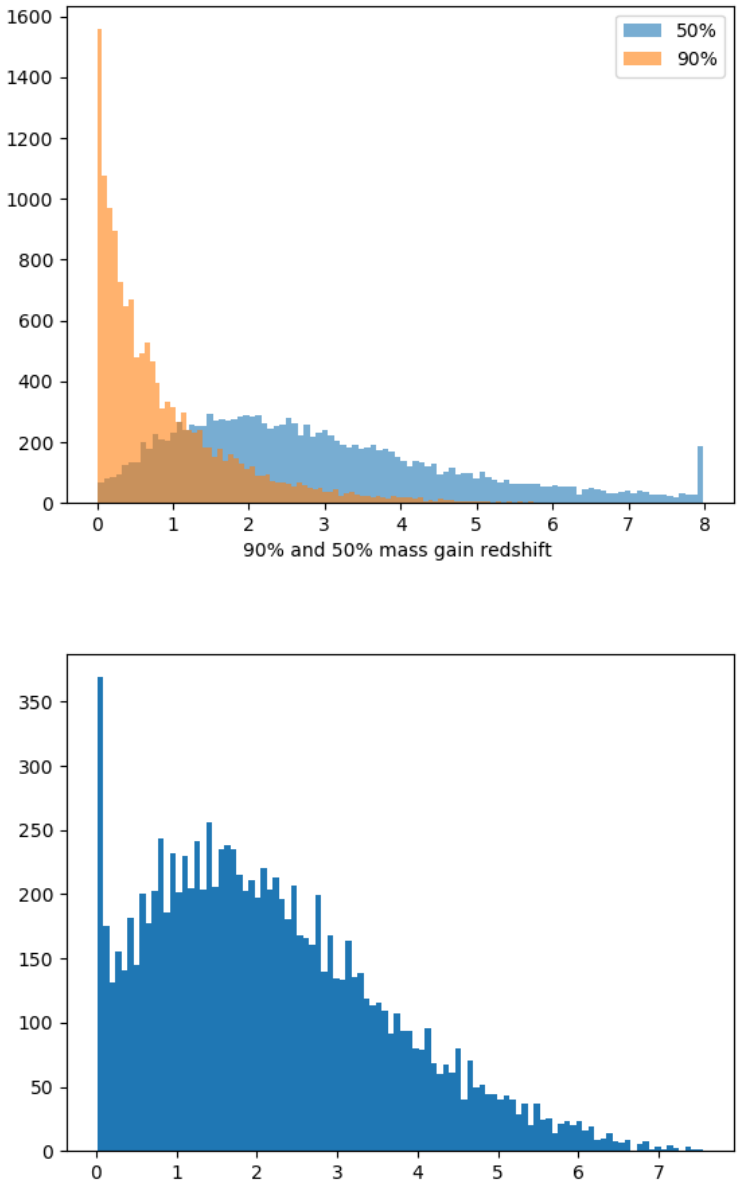

Figure 6: Up: histogram of redshifts of 50% and 90% mass gain redishift. Down: difference in 50% and 90% mass gain redshift

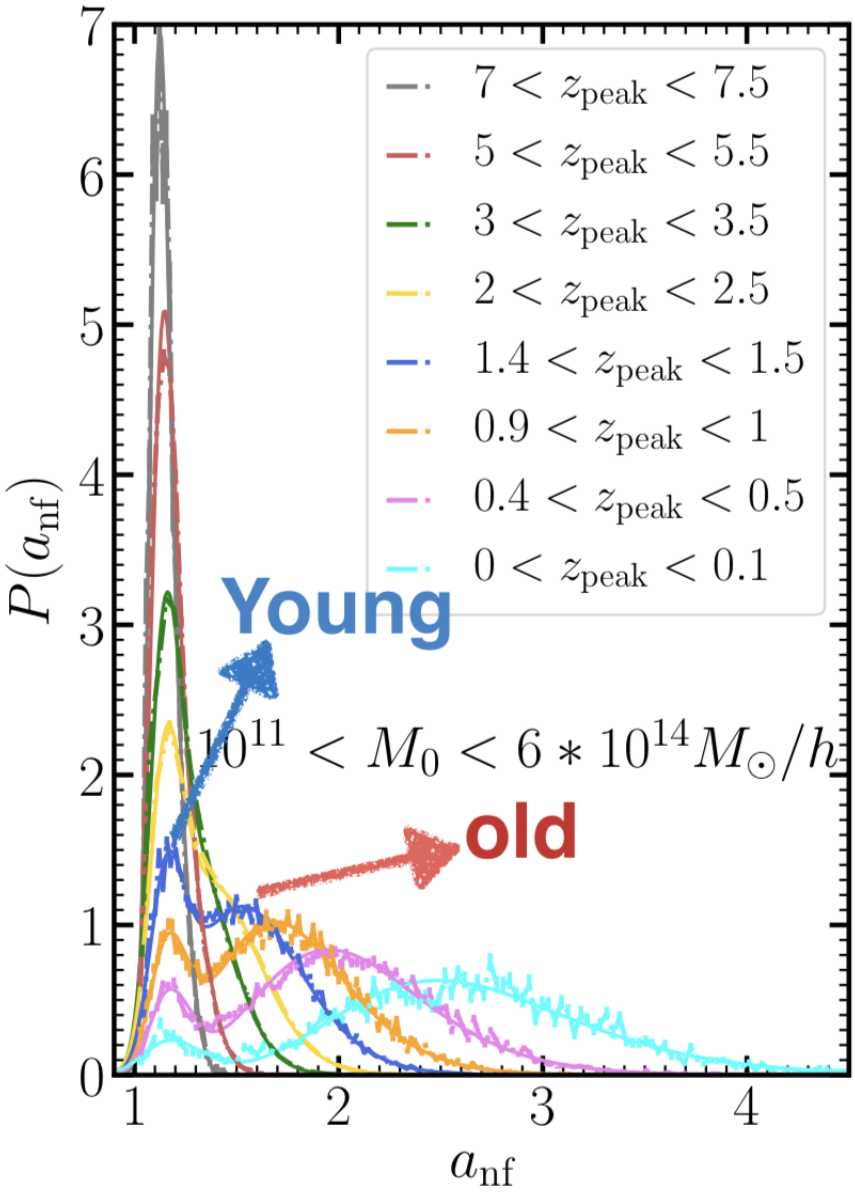

Figure 7: a_{nf} distribution plotted in (8) using N-body simulation. For halos that have their maxximum mass at lower redshifts, bimodality is clear.

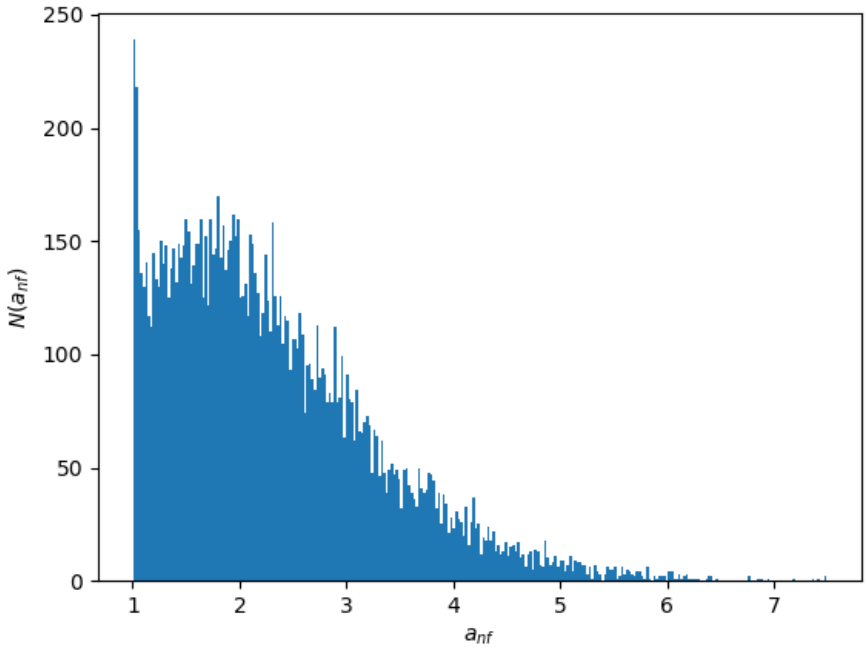

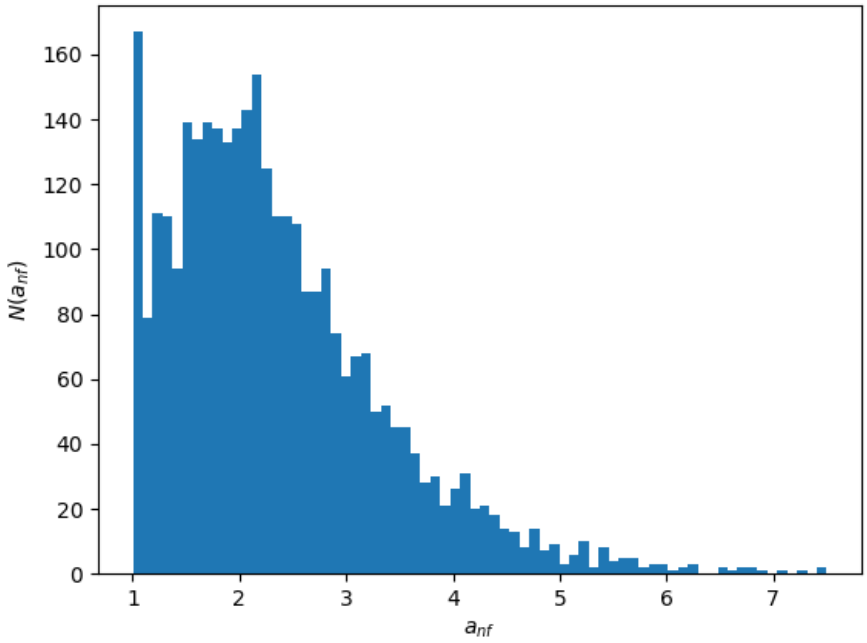

Figure 8: a_{nf} distribution for halos of mass $10^{13} M_{sun}$